Mechanical Systems and Signal Processing 104 (2018) 663–672

Contents lists available at ScienceDirect

Mechanical Systems and Signal Processing

journal homepage: www.elsevier.com/locate/ymssp

Parametric model of servo-hydraulic actuator coupled with a nonlinear system: Experimental validation

Amin Maghareh [a,*], Christian E. Silva [b], Shirley J. Dyke [b]

[a] Lyles School of Civil Engineering, Purdue University, West Lafayette, USA
[b] School of Mechanical Engineering, Purdue University, West Lafayette, USA

ARTICLE INFO

Article history:
Received 29 July 2017
Received in revised form 29 October 2017
Accepted 3 November 2017
Available online 29 November 2017

2010 MSC:
00-01
99-00

Keywords:
Hydraulic actuator
Transfer system
Control-structure interaction
Actuator modeling

ABSTRACT

Hydraulic actuators play a key role in experimental structural dynamics. In a previous study, a physics-based model for a servo-hydraulic actuator coupled with a nonlinear physical system was developed. Later, this dynamical model was transformed into controllable canonical form for position tracking control purposes. For this study, a nonlinear device is designed and fabricated to exhibit various nonlinear force-displacement profiles depending on the initial condition and the type of materials used as replaceable coupons. Using this nonlinear system, the controllable canonical dynamical model is experimentally validated for a servo-hydraulic actuator coupled with a nonlinear physical system.

1. Introduction

Hydraulic actuators are extensively used in structural control systems and for experimental testing to investigate the behavior of structural systems subjected to dynamic loads. However, researchers have demonstrated a natural velocity feedback which tightly couples the dynamic characteristics of a hydraulic actuator to the dynamics of the system to which it is attached [1,2]. Disregarding this coupling can severely limit both the performance and robustness of experiments and protective system [1,3]. For instance, in many active structural control situations, poor, or perhaps catastrophic, performance of the controlled system can occur due to the unmodeled or mismodeled dynamics of the actuator coupled with the structure [1]. Effective force testing methods have been found to be challenging due to a physical phenomenon known as *control-structure interaction* (CSI) in which the actuators attached to lightly damped structures have a significantly limited ability to apply control forces at the natural frequencies of the structure [1,4,5].

In most cases when hydraulic actuators are used for structural engineering purposes, success depends on the accurate application of forces or displacements to the structure (a.k.a. physical specimen). For instance, in *real-time hybrid simulation* (RTHS), hydraulic actuators serve as transfer system to enforce the interface conditions between the computational and physical substructures [6,3]. The first step to achieve accurate application of forces and displacements is to develop a model for hydraulic actuators (typical of those used in such structural testing) coupled with the physical specimen, see Fig. 1. Such a

* Corresponding author.
E-mail address: amaghare@purdue.edu (A. Maghareh).

https://doi.org/10.1016/j.ymssp.2017.11.009
0888-3270/

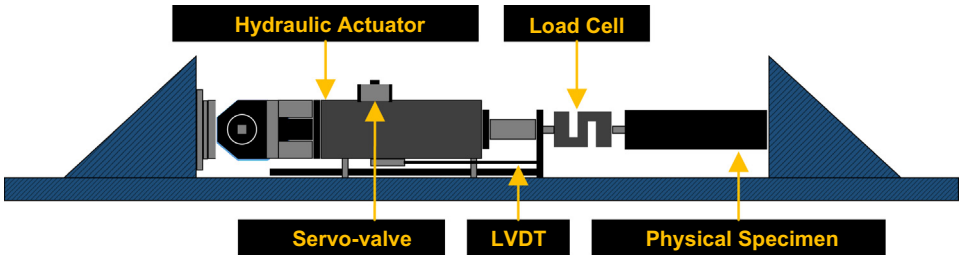

Fig. 1. Schematic diagram of a typical plant: a hydraulic actuator coupled with a general physical specimen with appropriate sensors.

model can be further used as a plant for designing controllers and compensators to enhance the accuracy of the forces or displacements to be provided by hydraulic actuators, therefore ensuring that their responses are as close as possible to the desired trajectories.

In this study, *plant* refers to the servo-hydraulic actuator coupled with the physical specimen. To develop a physics-based model for the plant, DeSilva linearized the fluid flow rate in the actuator about the origin [7]. In this linearized model, a natural velocity feedback path exists between the hydraulic actuator and the servo-valve input. The coupling between a hydraulic actuator and a physical specimen was explored by Dyke et al. [1]. In a set of experiments, they demonstrated that whenever a hydraulic actuator is attached to a linear physical specimen, the actuator has limited ability to apply forces at the natural frequencies of the physical specimen. Later, this model was extended to a nonlinear dynamical model for the case when a hydraulic actuator is coupled with a nonlinear physical specimen [3]. In addition, this dynamical model was further transformed to controllable canonical form for position tracking control purposes.

Controllability is a significant property of a control plant. Transforming the plant model into a controllable canonical dynamical model makes it appealing for displacement tracking. Adopting such model becomes especially important in two cases: (1) when control-structure interaction dominates the dynamics of the coupled system, and (2) when the hydraulic actuator is coupled with an unknown physical specimen (such as in the case of real-time hybrid simulation). In such cases, after identifying the parameters associated with the servo-hydraulic actuator [2,8], parametric and non-parametric uncertainties are incorporated in the model due to uncertainties in the physical specimen. The controllable canonical model is formulated so that the measured forces applied to the physical specimen are used as a feedback signal. Therefore, the measured force signal is used as an additional piece of information by the control law for accurate displacement tracking of the plant with a high level of uncertainty.

The objective of this study is to experimentally validate the controllable canonical dynamical model for nonlinear physical systems. For this purpose, a nonlinear specimen has been designed and fabricated, such that it has certain characteristics: (i) it exhibits a nonlinear force-displacement profile; (ii) it is a damage-controlled specimen and the damaged parts are easily replaceable (coupons); and (iii) various force-displacement profiles can easily be generated using different coupons.

2. Controllable canonical model

In [3], a nonlinear dynamical model was developed for a hydraulic transfer system coupled with a linear/nonlinear physical specimen. In addition, a simple technique was demonstrated to identify the parameters associated with the hydraulic system. A brief overview of this dynamical model is provided here. A block diagram representation of a typical servo-hydraulic actuator coupled with a nonlinear physical specimen is provided in Fig. 2.

Consider a single-degree-of-freedom nonlinear physical specimen, expressed in the generalized form

$$x_3 = h(x_1, x_2) + f/m, \tag{1}$$

where x_2 and x_3 denote $\dot{x}_1$ and $\ddot{x}_1$, respectively, and f and m are the actuator force and specimen mass, respectively. In [3], it was demonstrated that Fig. 2 can be reduced to the dynamically equivalent form shown in Fig. 3 which represents the

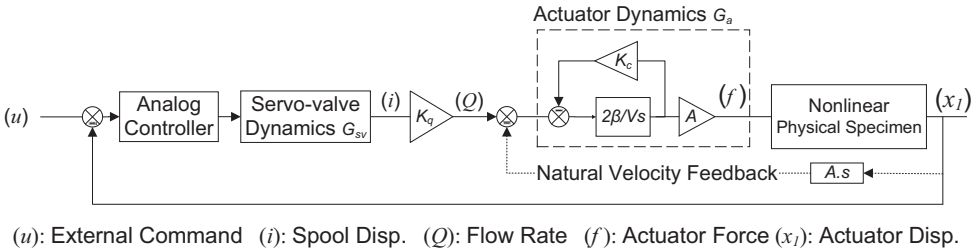

Fig. 2. General dynamics of the plant: a hydraulic actuator coupled with a nonlinear physical specimen.

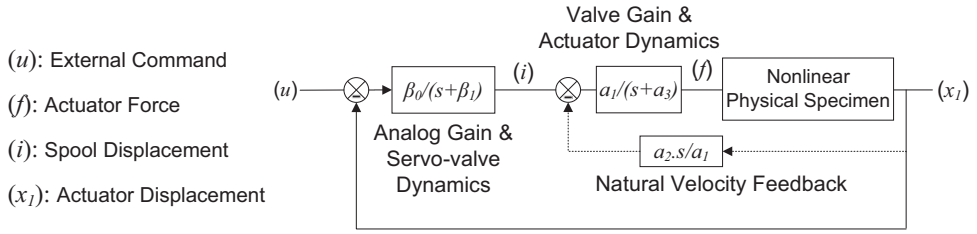

Fig. 3. Equivalent block diagram for the closed-loop plant.

dynamics from the external command (u) to the actuator displacement (x_1). The spool valve block, which represents *servo-valve dynamics* in Fig. 2, regulates the fluid flow rate (Q) to the hydraulic actuator and can be modeled as a first order transfer function [1,8,3,8]. However, it should be noted that the first order model is a simplified representation of the dynamics of servo-valve. For instance, for a servo-valve with the operational frequency bandwidth of 0–60 Hz, this simplified model may be able to capture the essential dynamics of the servo-valve up to ≈30 Hz. Further details on the dynamics of the electro-hydraulic servo-valve can be found in [10,11]. The first order model is given by

$$G(s) = \frac{\gamma}{s + \beta_1} \tag{2}$$

where γ and $1/\beta_1$ denote the constant gain and the servo-valve time constant, respectively.

To stabilize the plant, an analog PID controller is typically used. In this study, the integral (I) and derivative (D) gains are set to zero. In the model, the proportional (P) and γ are lumped into a new parameter, defined as

$$\beta_0 = P\gamma \tag{3}$$

With a simple rearrangement in Fig. 2, the actuator transfer function can be written as

$$G_a = \frac{A}{\frac{V}{2\beta}s + K_c} \tag{4}$$

and

$$K_q G_a = \frac{AK_q}{\frac{V}{2\beta}s + K_c} = \frac{\frac{AK_q}{K_c}}{\frac{V}{2\beta K_c}s + 1} \tag{5}$$

Table 1 describes the parameters associated with the plant model shown in Figs. 2 and 3.

Next, the parameters in Table 1 are lumped into three dummy parameters [1,2]: a_1, a_2, and a_3,

$$a_1 = \frac{2\beta K_q A}{V}; \quad a_2 = \frac{2\beta A^2}{V}; \quad a_3 = \frac{2\beta K_c}{V} \tag{6}$$

and substituting these into Eq. (5) yields

$$K_q G_a = \frac{\frac{a_1}{a_3}}{\frac{1}{a_3}s + 1} = \frac{a_1}{s + a_3} \tag{7}$$

The closed-loop plant in Fig. 3 is then written as a fourth order nonlinear system of differential equations:

Table 1
Hydraulic transfer system parameters.

Parameter	Units	Component	Description
P	mA/m	Analog Controller	Controller proportional gain
γ	m/mA/sec	Servo-valve	Servo-valve gain
$1/\beta_1$	sec	Servo-valve	Servo-valve time constant
K_q	m^3/sec/m	Servo-valve	Valve flow gain
i	m	Servo-valve	Spool displacement
A	m^2	Hydraulic actuator	Piston area
K_c	m^3/sec/Pa	Hydraulic actuator	Leakage coefficient of the actuator
V	m^3	Hydraulic actuator	Half the volume of the actuator
β	Pa	Hydraulic actuator	Effective bulk modulus of the fluid
Q	m^3/sec	Hydraulic actuator	Fluid flow rate into the actuator
x_1	m	Hydraulic actuator	Actuator displacement
f	N	Hydraulic actuator	Actuator force

$$\begin{cases} \dot{x}_1 &= x_2 \\ \dot{x}_2 &= h(x_1, x_2) + f/m \\ \dot{f} &= -a_2 x_2 - a_3 f + a_1 i \\ \dot{i} &= -\beta_0 x_1 - \beta_1 i + \beta_0 u \end{cases} \tag{8}$$

where u denotes the external command to the plant. The nonlinear dynamical model in Eq. (8) is transformed into a controllable canonical form shown in Eq. (9) [3]

$$\begin{cases} \dot{x}_1 &= x_2 \\ \dot{x}_2 &= x_3 \\ \dot{x}_3 &= x_4 \\ \dot{x}_4 &= -C_1 u + C_1 x_1 + C_2 x_2 + C_3 x_3 + C_4 x_4 + C_5 f + C_n \end{cases} \tag{9}$$

where

$$\begin{aligned} C_1 &= -a_1\beta_0/m \\ C_2 &= -\beta_1 a_2/m + \beta_1(\partial h/\partial x_1) + a_3(\partial h/\partial x_1) \\ C_3 &= \beta_1(\partial h/\partial x_2) + a_3(\partial h/\partial x_2) - a_2/m \\ C_4 &= -\beta_1 - a_3 \\ C_5 &= -\beta_1 a_3/m \end{aligned}$$

and

$$C_n = \ddot{h} = \frac{\partial^2 h}{\partial x_1^2} x_2^2 + \frac{\partial^2 h}{\partial x_2^2} x_3^2 + 2\frac{\partial^2 h}{\partial x_1 \partial x_2} x_2 x_3 + \frac{\partial h}{\partial x_1} x_3 + \frac{\partial h}{\partial x_2} x_4 \tag{10}$$

It should be noted that Eqs. (8) and (9) are dynamically identical [3].

Presenting a hydraulic actuator in the controllable canonical form gives a researcher an enormous advantage in terms of synthesizing an effective controller, especially if the plant behaves in a nonlinear manner. For precise displacement tracking, this dynamical model enables researchers to design an effective nonlinear controller. For example, Maghareh et al., developed a nonlinear controller (*Self-tuning Robust Control System, SRCSys*) which is based on this nonlinear dynamical model in controllable canonical form [12]. Further, in [3], this dynamical model was validated for linear SDOF systems, and the interaction present between the actuator and the physical specimen was studied in several linear experiments. In the next section, the validity of this model will be demonstrated experimentally for nonlinear physical specimens.

3. Experimental validation

To validate the controllable canonical model for a hydraulic actuator coupled with a nonlinear physical specimen, a nonlinear specimen is designed and fabricated (see Fig. 4). The nonlinear specimen is composed of a solid shaft that slides into a hollow shaft. These two pieces can be connected through two replaceable coupons subjected to yielding. This specimen is designed to have certain features: (i) it exhibits nonlinear force-displacement profile; (ii) the force-displacement profile can easily be modeled using Eq. (1); (iii) the force-displacement profile varies as functions of the initial condition of the

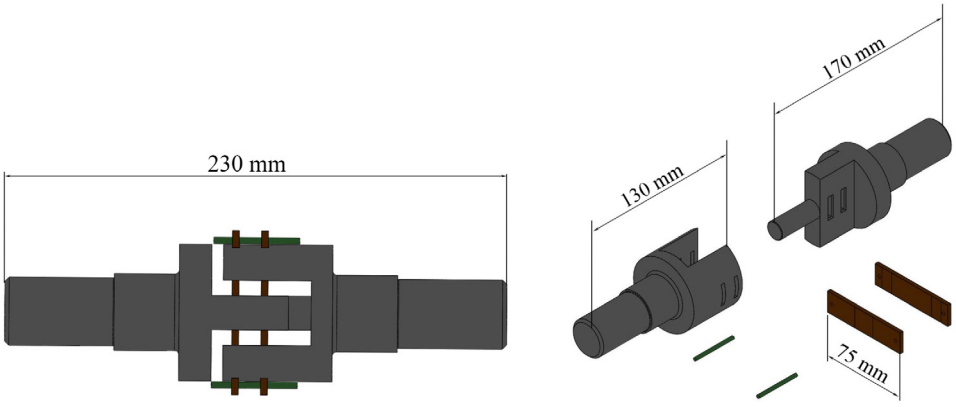

(a) Assembled View (b) Assembly View

Fig. 4. Physical specimen designed and fabricated for validation experiments.

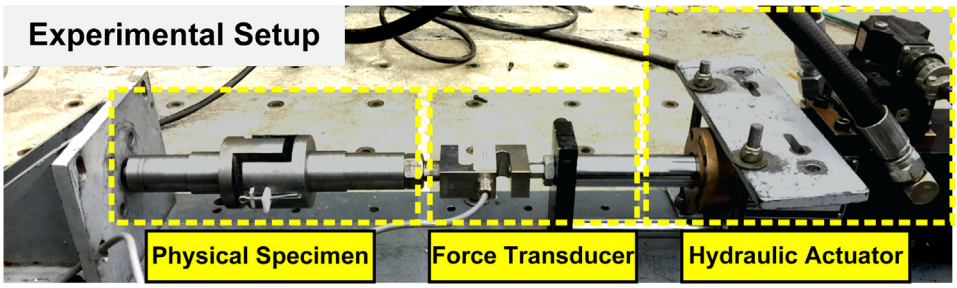

Fig. 5. Experimental setup: hydraulic actuator coupled with the nonlinear physical specimen.

specimen and the material used in the coupons (e.g., steel, aluminum, and brass); and (iv) after each experiment, the yielded part (the coupons) can be easily replaced.

The hydraulic actuator used in the experimental case studies is a ShoreWestern double-acting, double-ended dynamic actuator with product number 910D-.77-6-4-1348. The piston area for this actuator is $2.387 \times 10^{-4}\ \mathrm{m}^2$ and the actuator force capacity is 4.89 kN at 20.7 MPa pressure. A Schenck-Pegasus 162M servo-valve rated for 15 GPM at 20.7 MPa pressure is used to control the flow to the actuator. The servo-valve has a nominal operational frequency bandwidth of 0–60 Hz and is driven by the hydraulic controller. The actuator is placed in a small-scale loading frame located in the Intelligent Infrastructure Systems Laboratory, at Purdue University. The actuator in the loading frame is equipped with an internal LVDT displacement sensor. Control for this actuator is provided by a ShoreWestern SC6000 controller, which implements the analog PID control loop. It should be emphasized that in all experiments the integral (I) and derivative (D) gains are set to zero to agree with the modeling assumptions. The external command (u) is provided by a high-performance Speedgoat/xPC (Speedgoat GmbH, 2011) real-time kernel. High-resolution, high-accuracy, 18-bit analog I/O boards are integrated into this digital control system that supports up to 32 differential simultaneous A/D channels and eight D/A channels. A diagram of the experimental setup showing the servo-hydraulic actuator coupled with the nonlinear physical specimen is provided in Fig. 5.

The first step is to identify the parameters associated with the servo-hydraulic actuator. Although the hydraulic actuator is physically coupled with the physical specimen, a method has been developed to isolate and identify these parameters [3]. The parameters associated with the hydraulic actuator are identified only once prior to the experiments. These parameters do not vary as changes are made to the physical specimen. These parameters are provided in Table 2. Note that the only parameter in Table 2 that varies is $a_1\beta_0$ and it varies because it is linearly proportional to the (P) gain as shown in Eq. (3). The proportional (P) gain will intentionally be varied to validate the model in these experiments.

Four experiments are conducted while systematically varying the behavior of the physical specimen to thoroughly validate the dynamical model over a variety of operating conditions. The proportional (P) gain and the initial condition of the physical specimen are varied in these experiments to consider different scenarios. As mentioned previously, changes in the initial condition of the specimen generate different force-displacement profiles. The force generated by the specimen is estimated using a nonlinear least square (curve fitting) code in MATLAB as

$$f_n = m_n\ddot{x}_1 + h_n(x_1, \dot{x}_1) \tag{11}$$

where

$$h_n(x_1, \dot{x}_1) = c_n\dot{x}_1 + k_{n,1}x_1 + k_{n,2}x_1^2 + k_{n,3}x_1^3 \tag{12}$$

Note that the restoring force is estimated as a general third order polynomial function which is asymmetric with respect to the initial point. Based on the general behavior observed, this is suitable to capture the overall response. More complex models could be used with other types of nonlinearity, if necessary. In addition, Eq. (11) can easily be rearranged in the form of Eq. (1).

The experimental and estimated force-displacement profiles associated with Cases 1–4 (using Tables 2 and 3 and Eqs. 11 and 12) are shown in Fig. 6.

For each case study, the input (external) command takes the form

Table 2
Identified parameters associated with the hydraulic actuator.

Parameters	Values
β_1 [1/sec]	267
$a_1\beta_0$ [m Pa/sec^2]	$2.412 \times 10^9 \times P$
a_2 [m Pa]	7.881×10^5
a_3 [1/sec]	16.118

Table 3
Four experimental cases.

Case study	m_n (kg)	c_n (N sec/m)	$k_{n,1}$ (N/m)	$k_{n,2}$ (N/m^2)	$k_{n,3}$ (N/m^3)	P
Case 1 ($n=1$)	3	500	4.69×10^5	-7.52×10^6	2.44×10^{11}	2.0
Case 2 ($n=2$)	3	500	4.58×10^5	-3.86×10^8	2.35×10^{11}	2.5
Case 3 ($n=3$)	3	500	7.51×10^5	-5.88×10^8	2.34×10^{11}	3.0
Case 4 ($n=4$)	3	500	7.61×10^5	-5.78×10^8	2.18×10^{11}	3.5

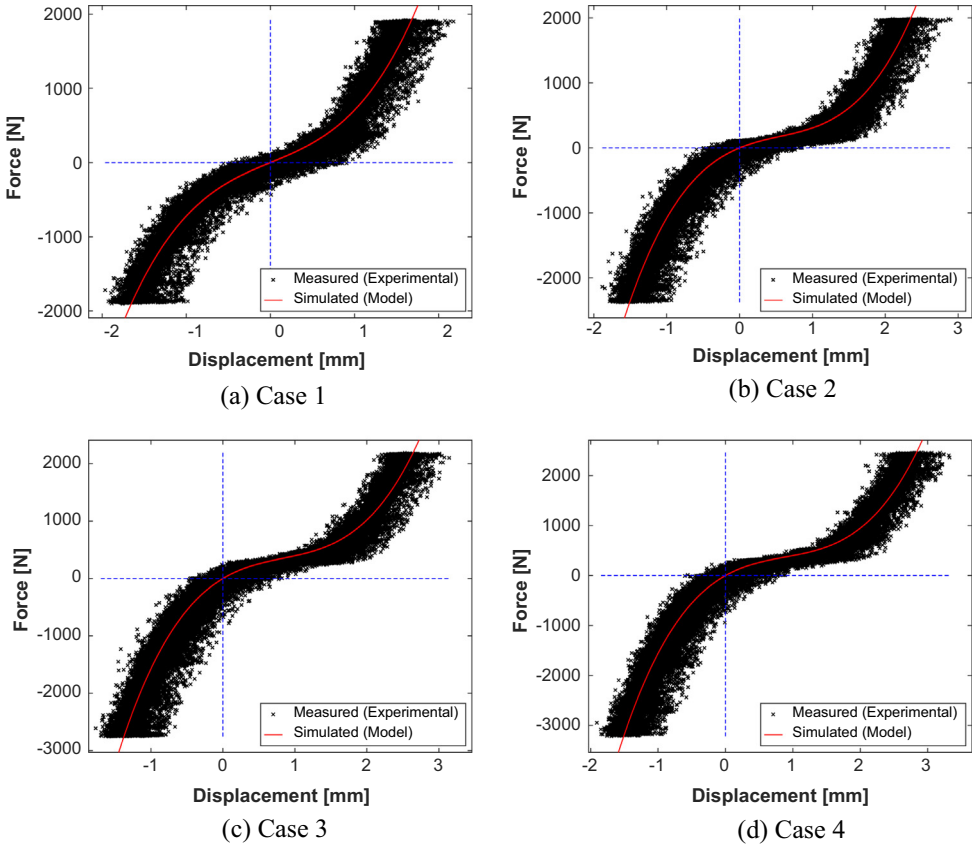

Fig. 6. Force-displacement profiles.

$$u(t) = A\sin(2\pi f_u t) \tag{13}$$

and the servo-hydraulic actuator coupled with the nonlinear physical specimen is tested for $A = 6$ mm and f_u is set to either 1 Hz or 10 Hz. In this study, to quantify the modeling error corresponding to the dynamical model in Eq. (9), the following normalized error is used

$$NE = \frac{\sqrt{\frac{1}{N}\sum_{i=1}^{N}(x_i^p - x_i^e)}}{\max(|x_i^e|)} \times 100 \tag{14}$$

where N, x_1^p and x_1^e correspond to number of sample points, estimated displacement and experimental displacement, respectively.

Fig. 7 shows the measured responses associated with Cases 1–4. The command amplitude and frequency in Fig. 7a are 6 mm and 1 Hz, respectively. In Fig. 7b, the command amplitude and frequency are 6 mm and 10 Hz, respectively. Figs. 6 and 7 clearly demonstrate the impact of asymmetric force-displacement behavior of the physical specimen on the actuator's response.

To demonstrate the accuracy of the dynamical model, Figs. 8–11 compare the experimental and simulated responses where $u(t)$ is the input command. Fig. 8 corresponds to Case Study 1 with the displacement-force profile shown in Fig. 6a and the proportional (P) gain set to 2 mA/m. In Fig. 8a and b, the command frequency is $f_u = 1$ Hz and in Fig. 8c and d,

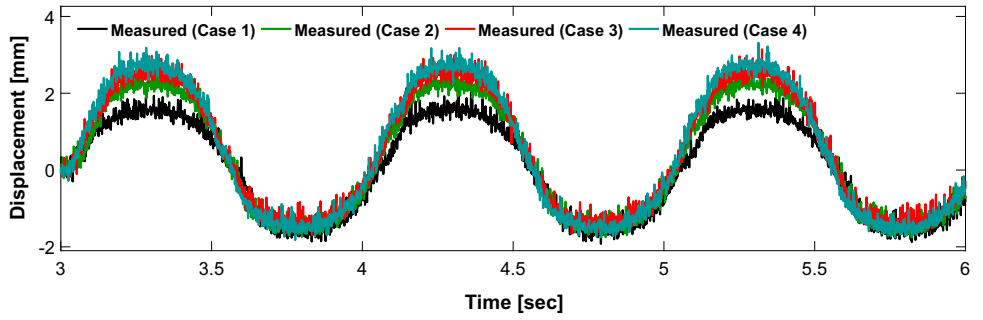

(a) $f_u = 1$ Hz

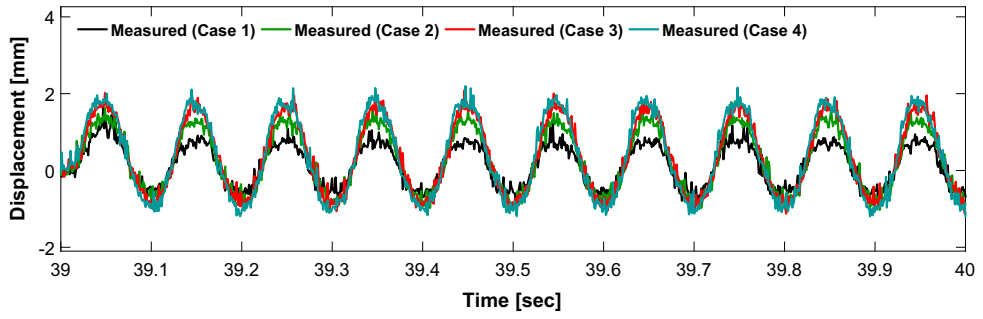

(b) $f_u = 10$ Hz

Fig. 7. Case Studies 1–4: comparison of the experimental responses.

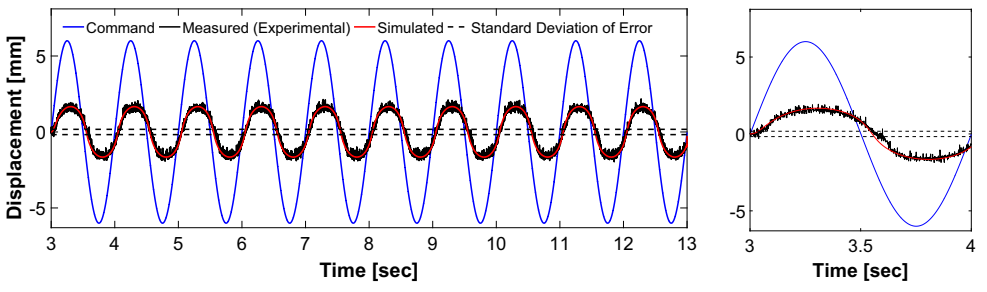

(a) $f_u = 1$ Hz (b) $f_u = 1$ Hz

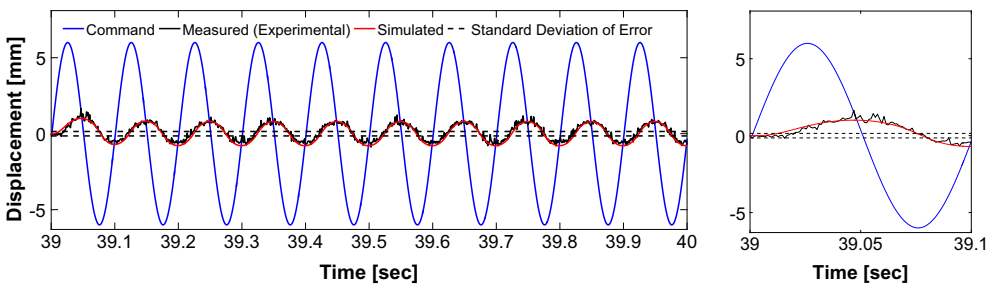

(c) $f_u = 10$ Hz (d) $f_u = 10$ Hz

Fig. 8. Case Study 1: comparison of the experimental and simulated responses.

the command frequency is $f_u = 10$ Hz. The corresponding normalized errors for these two experiments are *NE* = 7.97% and *NE* = 8.88%. Fig. 9 corresponds to Case Study 2 with the displacement-force profile shown in Fig. 6b and the proportional (*P*) gain set to 2.5 mA/m. Fig. 10 refers to Case Study 3 with the displacement-force profile shown in Fig. 6b and the proportional (*P*) gain set to 3 mA/m.

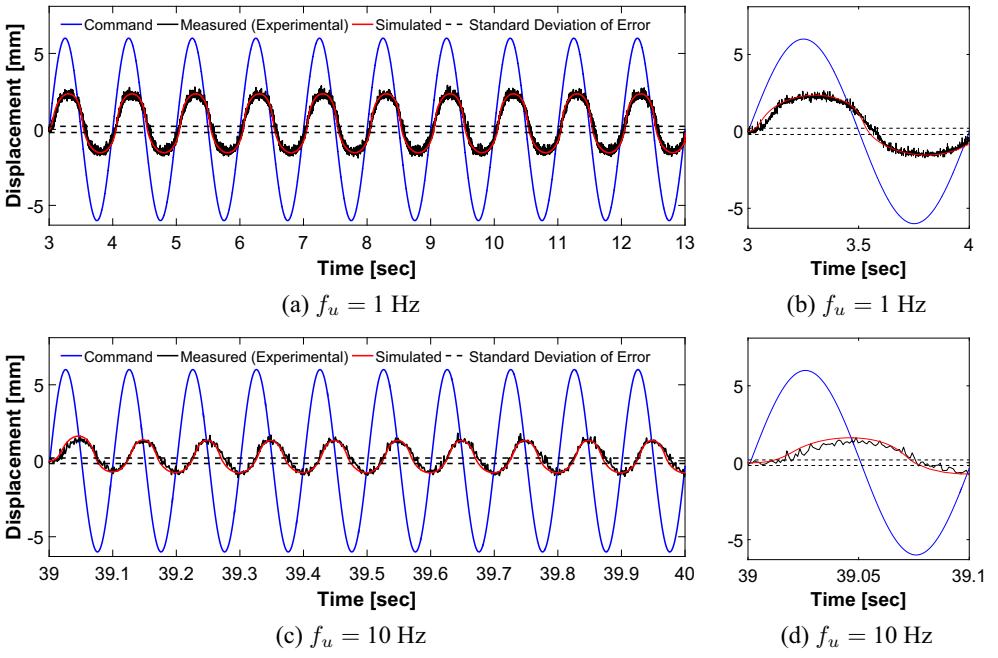

(a) $f_u = 1$ Hz (b) $f_u = 1$ Hz

(c) $f_u = 10$ Hz (d) $f_u = 10$ Hz

Fig. 9. Case Study 2: comparison of the experimental and simulated responses.

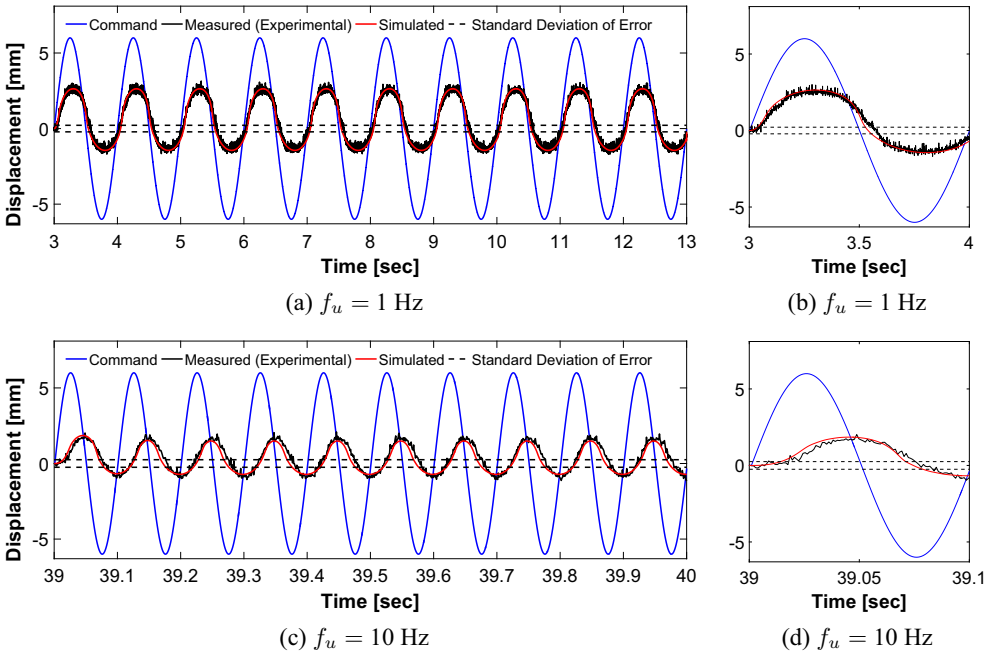

(a) $f_u = 1$ Hz (b) $f_u = 1$ Hz

(c) $f_u = 10$ Hz (d) $f_u = 10$ Hz

Fig. 10. Case Study 3: comparison of the experimental and simulated responses.

In Figs. 9a and 10a, the frequency of command inputs is $f_u = 1$ Hz; and in Figs. 9c and 10c, the frequency of command inputs is $f_u = 10$ Hz. The normalized errors corresponding to Figs. 9a, c, 10a and c are *NE* = 7.01%, *NE* = 9.54%, *NE* = 6.89% and *NE* = 10.96%, respectively. Fig. 11 corresponds to Case Study 4 with the displacement-force profile shown in Fig. 6d and the proportional (P) gain is set to 3.5 mA/m. In Fig. 11a, the command frequency is $f_u = 1$ Hz, and in Fig. 11c the command frequency is $f_u = 10$ Hz. The corresponding normalized errors for these two experiments are *NE* = 6.39% and *NE* = 10.76%.

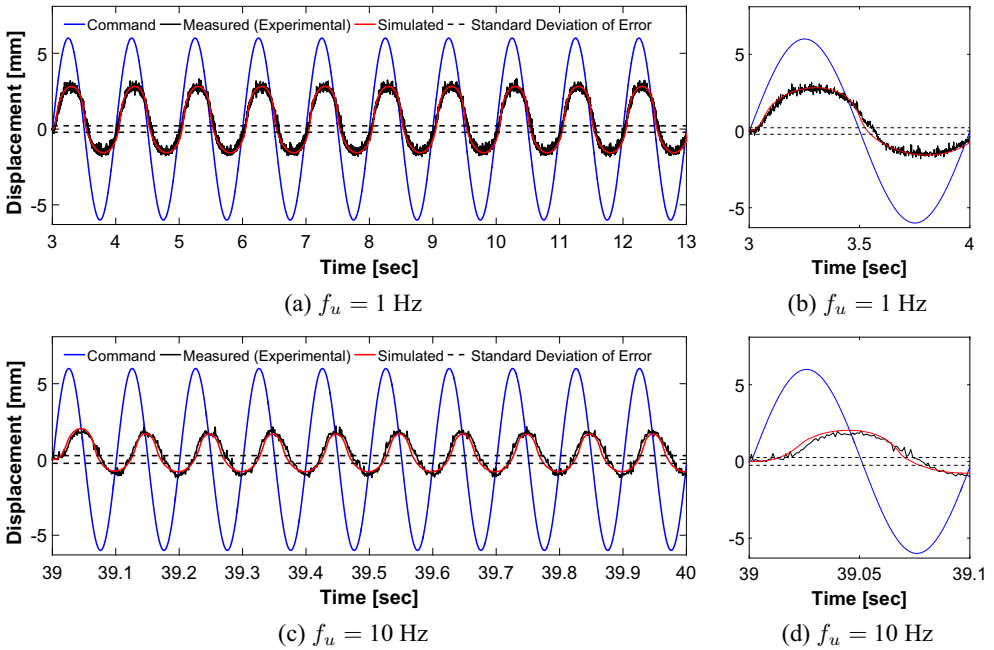

Fig. 11. Case Study 4: comparison of the experimental and simulated responses.

In addition to Cases 1–4, similar experiments with $f_u = 3$ Hz and $f_u = 5$ Hz are conducted. The corresponding experimental normalized errors are provided in Fig. 12.

The time domain comparisons and the corresponding normalized errors, provided in Fig. 12, show good agreement between the experimental and simulated responses. It should be noted that 3–5% of the normalized errors in these experiments are due to the measurement noise present in the LVDT reading (which are measured in the case of no external command).

From Fig. 12, it is observed that minimum modeling error is obtained when the proportional (P) gain = 1 mA/m. This observation can be related to the range of validity/accuracy of the linear model adopted for the hydraulic actuator and the servo-valve. It should be mentioned that the parameters in Table 2 were identified while the (P) gain was set to 1 mA/m. One underlying assumption of these linear models is that when the servo-hydraulic actuator parameters (such as the proportional gain) and input command vary, the actuator behaves in a linear fashion. Thus, the slightly larger errors associated with different values of the proportional (P) gain can be related to the range of validity/accuracy of this assumption and within a reasonable range of operation, these errors can be incorporated into the dynamical model as parametric uncertainties. In addition, another possible source of error, which can dictate the range of accuracy of this dynamical model, is the simplified first order model used to represent the dynamics of the servo-valve.

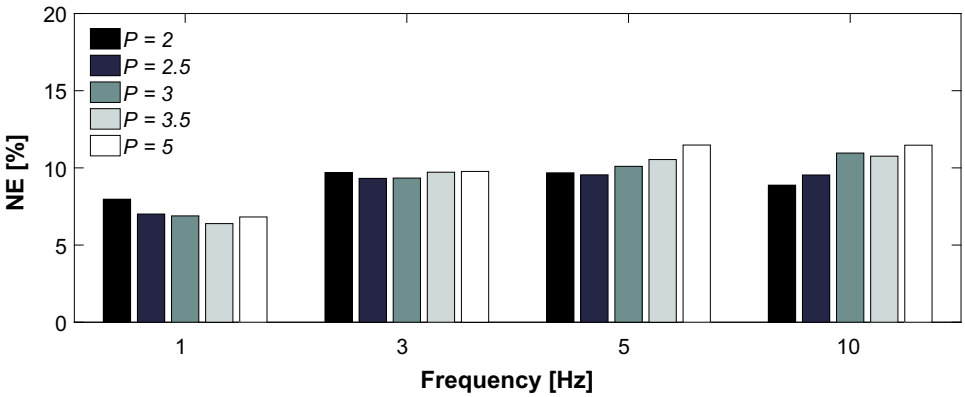

Fig. 12. Normalized errors associated with different experiments.

4. Conclusion

A controllable canonical dynamical model for a servo-hydraulic actuator coupled with a nonlinear physical system has been experimentally validated. For this purpose, a damage-controlled nonlinear device was designed and fabricated. The parameters associated with the hydraulic actuator have been decoupled and identified. In a series of experiments, the dynamical model has been validated for a range of different operating conditions subjected to sinusoidal input commands (from 1 Hz to 10 Hz). Time-domain comparisons and normalized errors associated with these experiments were provided in the results section. The comparisons show good agreement between the experimental and model responses (6% to 11% from which 3% to 5% correspond to measurement noise). For many experimental applications, highly-accurate position tracking of hydraulic actuator is required. For these applications, the controllable canonical dynamical model can serve as the control plant to design a nonlinear controller and enhance the performance and stability of the hydraulic actuator coupled with a nonlinear system.

Acknowledgment

This material is based in part upon work supported by the NSF under grant CNS-1136075 and the National Secretariat for Higher Education, Science, Technology and Innovation of Ecuador (SENESCYT). In addition, the writers would like to express their appreciation to the support for the development of the novel CIRST instrument made possible through the NSF MRI Program under grant CNS-1028668 and the School of Mechanical Engineering at Purdue University.

References

[1] S.J. Dyke, B.F. Spencer Jr, P. Quast, M.K. Sain, Role of control-structure interaction in protective system design, J. Eng. Mech. 121 (2) (1995) 322–338, https://doi.org/10.1061/(ASCE)0733-9399(1995)121:2(322).
[2] A. Maghareh, C.E. Silva, S.J. Dyke, Servo-hydraulic actuator in controllable canonical form: identification and experimental validation, Mech. Syst. Signal Process. 100 (2018) 398–414, https://doi.org/10.1016/j.ymssp.2017.07.022.
[3] B.M. Phillips, B.F. Spencer, Model-based multiactuator control for real-time hybrid simulation, J. Eng. Mech. 139 (2) (2013) 219–228, https://doi.org/10.1061/(ASCE)EM.1943-7889.0000493.
[4] J. Dimig, C. Shield, C. French, F. Bailey, A. Clark, Effective force testing: a method of seismic simulation for structural testing, J. Struct. Eng. 125 (9) (1999) 1028–1037, https://doi.org/10.1061/(ASCE)0733-9445(1999)125:9(1028).
[5] N. Nakata, Effective force testing using a robust loop shaping controller, Earthq. Eng. Struct. Dyn. 42 (2) (2013) 261–275, https://doi.org/10.1002/eqe.2207.
[6] X. Shao, A.M. Reinhorn, M.V. Sivaselvan, Real-time hybrid simulation using shake tables and dynamic actuators, J. Struct. Eng. 137 (7) (2011) 748–760, https://doi.org/10.1061/(ASCE)ST.1943-541X.0000314.
[7] C.W. de Silva, Control Sensors and Actuators, Taylor & Francis Group, LLC, Broken Sound Parkway, NW, 2007.
[8] Y. Qian, G. Ou, A. Maghareh, S.J. Dyke, Parametric identification of a servo-hydraulic actuator for real-time hybrid simulation, Mech. Syst. Signal Process. 48 (1–2) (2014) 260–273. https://doi.org/10.1016/j.ymssp.2014.03.001.
[9] J.E. Carrion, B.F. Spencer, Model-based Strategies for Real-time Hybrid Testing (December).
[10] D.H. Kim, T. Tsao, A linearized electrohydraulic servovalve model for valve dynamics sensitivity analysis and control system design, J. Dyn. Syst. Meas. Contr. 122 (1) (2000) 179, https://doi.org/10.1115/1.482440.
[11] A. Plummer, Control techniques for structural testing: a review, Proc. Inst. Mech. Eng. Part I: J. Syst. Control Eng. 221 (2) (2007) 139–169, https://doi.org/10.1243/09596518JSCE295.
[12] A. Maghareh, S.J. Dyke, C.E. Silva, Self-tuning robust control system for real-time hybrid simulation with highly uncertain nonlinear physical substructure, Struct. Control Health Monit. (2017) (submitted for publication).